Reliable High Impedance Fault Detection with Experimental Investigation in Distribution Systems

Mostafa Satea
Department of Building and Construction Techniques Engineering, Technical College Musayyib, Al Furat Al Awsat Technical University, Iraq
mustafasatea894@gmail.com

Mahmoud Elsadd
Electrical Engineering Department, College of Engineering, Damanhour University, Egypt
mahmoud.elsadd@dmu.edu.eg

Mohamed Zaky
Department of Electrical Engineering, College of Engineering, Northern Border University, Arar, 1321, Saudi Arabia
mohamed.zaky@nbu.edu.sa (corresponding author)

Mahmoud Elgamasy
Electrical Engineering Department, Faculty of Engineering, Menoufia University, 32511, Shebin Elkom, Egypt
mahmoud.elgamasy@sh-eng.menofia.edu.eg

Received: 3 July 2024 | Revised: 17 August 2024 | Accepted: 29 August 2024

Licensed under a CC-BY 4.0 license | Copyright (c) by the authors | *DOI: https://doi.org/10.48084/etasr.8292*

ABSTRACT

An approach for high-impedance fault detection is introduced in this paper. This technique discriminates between high-impedance faults and switching conditions by utilizing changes in the third harmonic current/voltage magnitude in conjunction with the conventional wavelet algorithm. The concept of discrimination is based on the observation that switching conditions typically do not involve changes in the zero-sequence third harmonic magnitude. However, in the case of high-impedance arcing faults, a noticeable change in the third harmonic current or voltage magnitude occurs. The performance of the proposed technique is examined through a detailed simulation of an actual medium voltage radial distribution feeder. In this simulation, high-impedance faults are represented by an arc model. The simulation, conducted in MATLAB for different fault cases, reveals that all fault cases are detected using the proposed technique. Furthermore, the experimental validation of the reliability of the proposed technique is accomplished using the same actual distribution feeder.

Keywords-recursive Fourier transform; discrete wavelet transform; high impedance faults; MV network

I. INTRODUCTION

Distribution systems frequently encounter both permanent and temporary faults, with temporary faults being the most prevalent, constituting over 80% of all faults. Various types of faults can occur, including phase faults involving two or more different conductors, as well as ground faults involving one or more conductors to ground. Ground faults may arise due to fallen conductors, resulting in permanent single or double phase-to-ground faults, thus making earth faults the most frequent fault in the system. High Impedance Faults (HIFs) are characterized by undesirable electrical contacts between a bare energized conductor and a non-conducting foreign object. Non-conductors inherently present high impedances to current flow due to their material characteristics. Typically, HIFs occur when a conductor physically breaks and falls onto a high-impedance surface, such as an asphalt road, sand, grass, or a tree, posing significant threats to both human life and the environment [1, 2]. Another common type of HIF occurs when the conductor remains intact but comes into contact with non-conducting grounded objects, often due to failures in the conductor mounting system, insulation failure, or inadvertent

contact with external elements such as tree limbs, vegetation, or walls [3, 4,]. These faults typically exhibit arcing signatures similar to those of broken conductors lying on the ground. In multi-grounded distribution lines, imbalances in three-phase loads are common, leading to overcurrent ground relays being set somewhat high to accommodate large neutral currents resulting from this imbalance [5]. In [6], a HIF detection method is described that monitors power polarity by multiplying the Discrete Wavelet Transform (DWT) detail coefficients of phase voltage and current for each feeder. In [7], the HIF detection in transmission systems is achieved using the maxima of the zero-sequence signals with the Wavelet Transform (WT). In [8, 9], the proposed HIF detection approach for distribution networks uses machine learning to enhance security against load switching. In [10], a HIF detection method for power distribution networks uses mathematical morphology to extract features from current signals in the time domain. In [5, 11, 12], an overview of HIF detection approaches is provided. However, finding a reliable HIF technique that combines high dependability with security against normal transients, such as high load switching, remains a significant challenge for protection engineers.

The primary contribution of this paper is in addressing the limitations of the conventional DWT algorithm in detecting HIFs. The conventional DWT algorithm struggles to differentiate between normal switching events and high impedance faults. To enhance the security of the proposed approach, a new criterion is introduced. This additional criterion is based on monitoring the variation in the third harmonic magnitude of the zero-sequence voltage and current. The Discrete Fourier Transform (DFT) is employed to extract the features of the harmonic components by estimating the associated third harmonic phasors for the zero sequence components of voltage and current waveforms, which are then input into another classifier. Simulation and computation were conducted using the MATLAB package, utilizing actual modeling data from a typical 11 kV feeder in the Egyptian network (Shebin El-Kom, Menoufia, Egypt), considering various conditions such as fault inception angle, fault resistance, and fault location. Furthermore, the experimental validation of the reliability of the proposed technique is accomplished utilizing the same actual distribution feeder.

II. PROPOSED FAULT DETECTION TECHNIQUE

The proposed approach detects HIFs by employing two criteria to ensure both sensitivity and security. The first criterion relies on monitoring the absolute sum value of the first detail output (D1 components) obtained from DWT over a single cycle period (*Sum_D1*). Sampling occurs at a rate of 1600 Hz, equivalent to 32 samples per cycle at 50 Hz. The approach employs a moving window strategy, continuously shifting the one-cycle window of DWT output by one sample. To indicate a high-value output signal for this characteristic, *Sum_D1* must persistently surpass a predefined threshold level, *M*, for a designated period or for *N* consecutive samples following the occurrence of a fault, as outlined in the right-hand side of the flowchart depicted in Figure 1 where *i* serves as a counter representing the sample number and thereby delineating the time interval containing information pertaining to the presence of HIF. Three categories of mother wavelets are employed in signal processing to pinpoint an optimal wavelet family for accurately detecting HIFs. These mother wavelets are Daubechies (db 14), coiflets (coif 4), and biorthogonal (bior 3.1). To choose the most appropriate mother wavelet, we adopt the maximum sum value of D1 coefficients over a single cycle period at the power frequency through wavelet analysis. On the other hand, the second criterion involves monitoring the third harmonic of zero-sequence current and voltage components at the primary substation of the distribution network. These components are derived by applying DFT to the estimated instantaneous zero-sequence current and voltage components. Essentially, this criterion relies on averaging the recent third harmonic magnitude of zero-sequence voltage and current waveforms over time and storing these values for comparison. Upon the occurrence of a fault, the new third harmonic magnitudes for voltage and current waveforms, respectively, are subtracted from the stored values. If the resulting magnitude continuously surpasses a preset threshold level for a predefined period or for *N* samples following the initiation of the fault, as depicted on the right-hand side of the flowchart in Figure 1, a HIF is declared.

III. SIMULATED SYSTEM AND HIF MODEL

An actual distribution feeder in the Egyptian distribution system is simulated. The feeder has a 66/11 kV delta/star-earthed primary transformer. Distributed loads along the feeder are fed by 11/0.4 kV load transformers, as shown in Figure 2. The details of the chosen distribution feeder are listed in [1]. The HIF represented in this study, as shown in Figure 3, involves an energized conductor in contact with a high impedance ground. The model used here is derived from the Kizilcay arc description, which relies on energy balance within the arc [13]. It is defined by:

$$\frac{dg}{dt} = \frac{1}{\tau} \cdot (G - g) \tag{1}$$

where τ represents the arc time constant, g denotes the instantaneous arc conductance, and G stands for the stationary arc conductance, characterized by:

$$G = \frac{|i_{arc}|}{U_O + r_o \cdot i_{arc}} \tag{2}$$

In this context, i_{arc} represents the instantaneous arc current, u_0 signifies the characteristic arc voltage, and r_0 denotes the characteristic arc resistance. The parameters u_0, r_0, and τ depend on the arc length (l_{arc}) are computed using the following equations derived from the arc measurements:

$$U_O = 0.9\ (kV/m) \cdot l_{arc} + 0.4\,(kV) \tag{3}$$

$$r_O = 40\ (m\Omega/m) \cdot l_{arc} + 8\,(m\Omega) \tag{4}$$

$$\tau = \tau_0 \cdot \left(\frac{l_{arc}}{l_0} \right)^{\alpha} \tag{5}$$

where τ_0 represents the initial time constant, l_0 signifies the initial arc length, and α denotes the coefficient with a negative value.

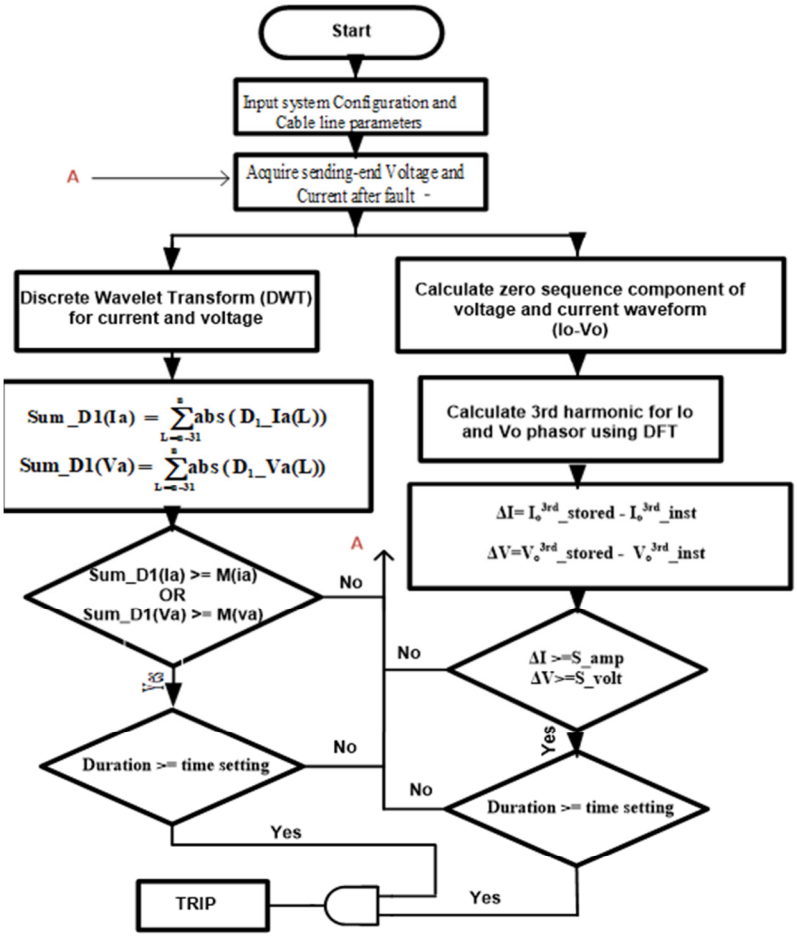

Fig. 1. Flowchart of the HIF fault detection algorithm.

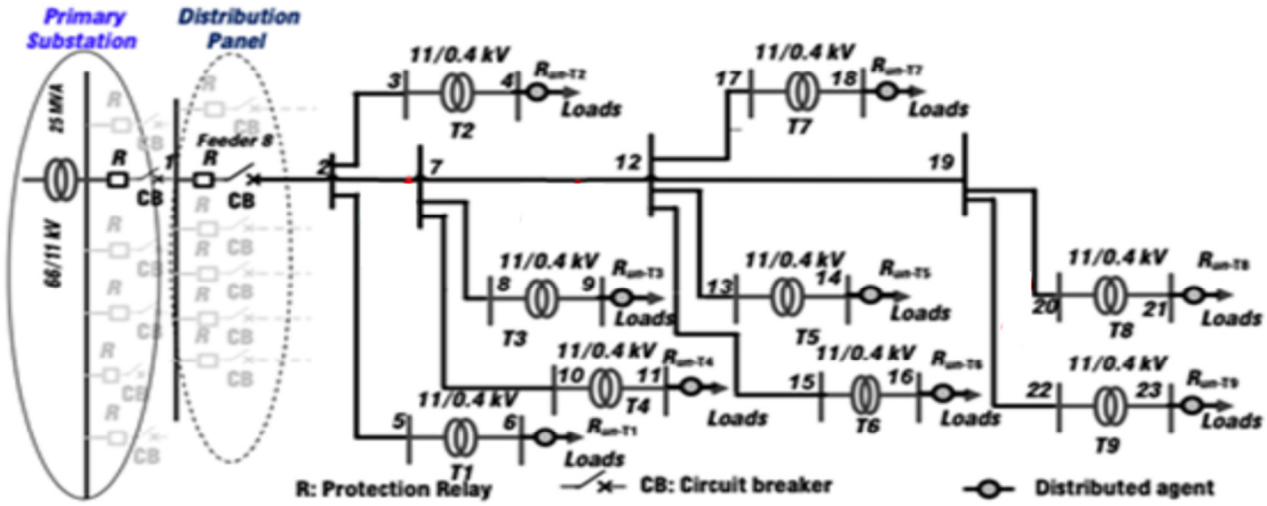

Fig. 2. Schematic of the selected distribution feeder.

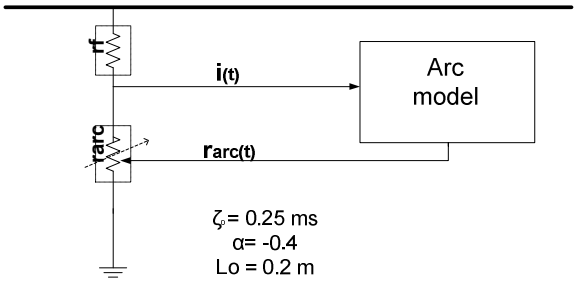

Fig. 3. Arc model structure.

A HIF was simulated at 5.53 km from the substation. The fault occurred at time 60 ms and persisted for 140 ms, completing seven cycles before being cleared by isolating the faulted phase. Figure 4 depicts the waveforms of fault current and voltage recorded at the relaying point, utilizing current and voltage transformers with ratios of 5:100 and 110:11000, respectively. The time-varying arc conductance associated with this fault is presented in Figure 5.

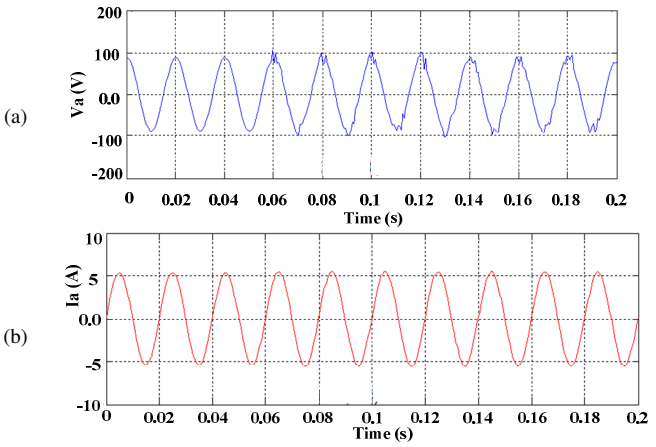

Fig. 4. Measured data at relay point under HIF at 5.53 km. (a) Voltage waveform, (b) current waveform.

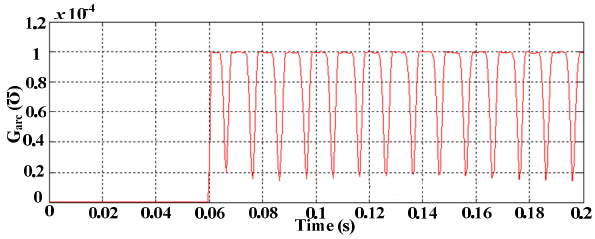

Fig. 5. Time-varying arc conductance of the arc modeled at 5.53 km.

IV. VALIDATION RESULTS

The Daubechies mother wavelet of order 14 (db14) is chosen to scrutinize the voltage and current waveforms. A multitude of testing scenarios was devised and executed to evaluate the performance of the HIF detection algorithm. MATLAB signals representing HIFs occurring at different locations and with varying inception angles were collected. Furthermore, the voltage waveforms resulting from non-fault disturbances in the power system, such as load switching, were analyzed to assess the security of the algorithms.

A. High Impedance Ground Faults on Feeders - Contact Grounded Objects

Figure 6 shows the three-level wavelet analysis of voltage and current waveforms at the relay point for a fault occurring 5.53 km from the utility bus at a 90° fault inception angle. The analysis of Figure 6 confirms that the first detail (D1) component is the most suitable for identifying HIFs, and therefore, it was selected. Figure 7 displays the variations in the summed values of the D1 coefficients of voltage and current waveforms at the relay point for an HIF at 6.48 km. Additionally, Figures 8 and 9 present the variations in the third harmonic of the zero-sequence components of voltage and current waveforms during the same fault. Figure 10 illustrates the variation profiles of the summed values of the D1 coefficient of voltage and current waveforms as a function of both the fault distance and the number of samples (running time) with 1000 Ω Rf. It can be concluded that the minimum summed values of voltage and current waveforms are 91.5 V and 0.939 A, respectively.

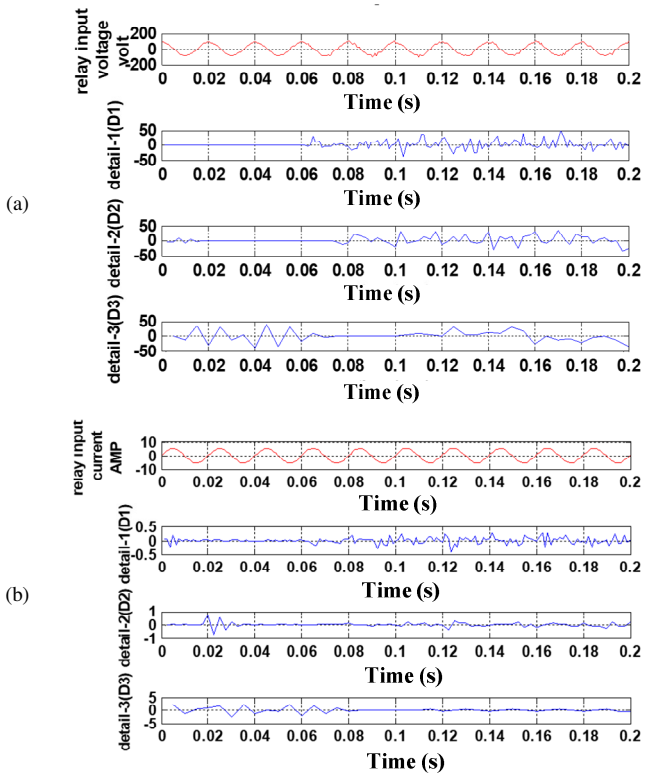

Fig. 6. Wavelet decomposition of the measured (a) voltage and (b) current waveforms.

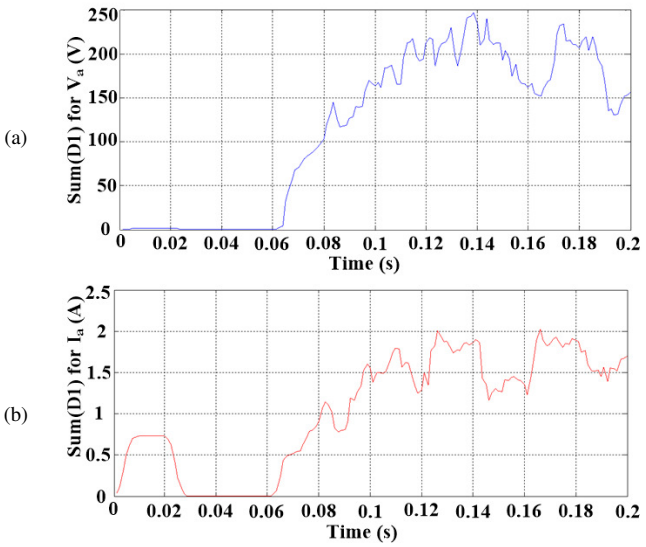

Fig. 7. Variation of the summated values of coefficient D1 of (a) voltage and (b) current waveforms at the relay point for HIF at 6.48 km.

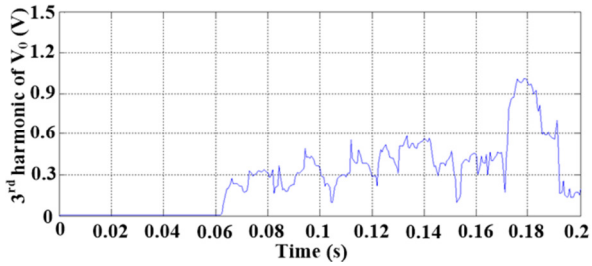

Fig. 8. Variation of the 3rd harmonic of the zero sequence component of the voltage waveform at the relay point for HIF at 6.48 km.

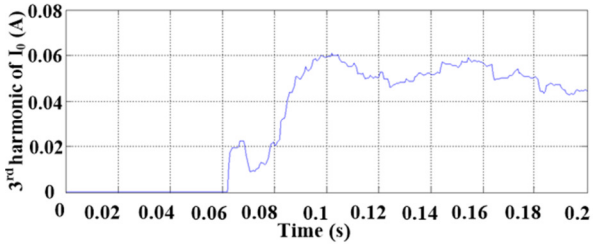

Fig. 9. Variation of the 3rd harmonic of the zero sequence component of the current waveform at the relay point for HIF at 6.48 km.

Figure 11 depicts the variation profile of the third harmonic of the zero-sequence components of voltage and current waveforms as a function of both the fault distance and the number of samples (running time) with 1000 Ω *Rf*. One can conclude that the minimum differences between the new third harmonic magnitudes for voltage and current waveforms during HIF and the average value of the third harmonic magnitudes for zero-sequence components of voltage and current waveforms pre-fault are 0.163 V and 0.038 A, respectively. In all the above mentioned cases, the voltage at the relay point is recorded for 0.2 s, divided into 0.06 s (three cycles for a 50 Hz system) before fault inception and 0.14 s (7 cycles for a 50 Hz system) after fault inception.

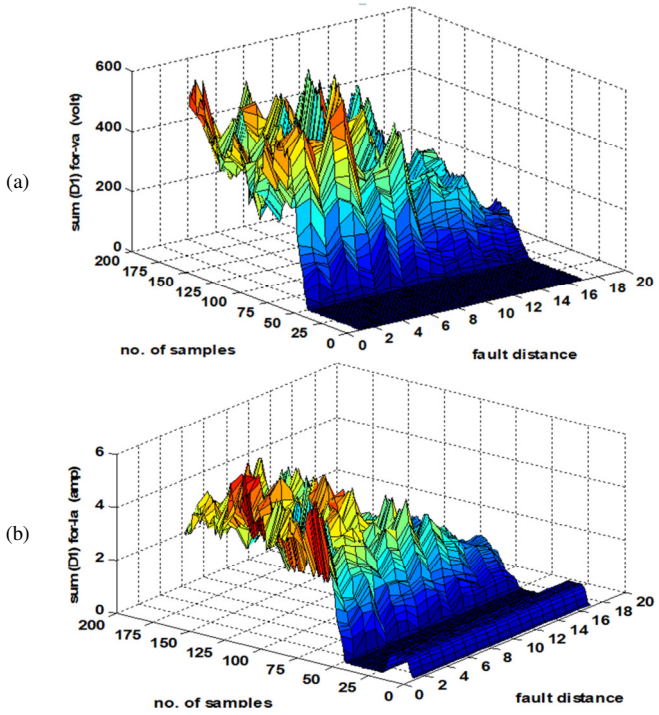

Fig. 10. Performance profile of the absolute sum values of coefficient D1 of (a) voltage waveform (b) current waveform for HIF with 1000Ω *Rf*.

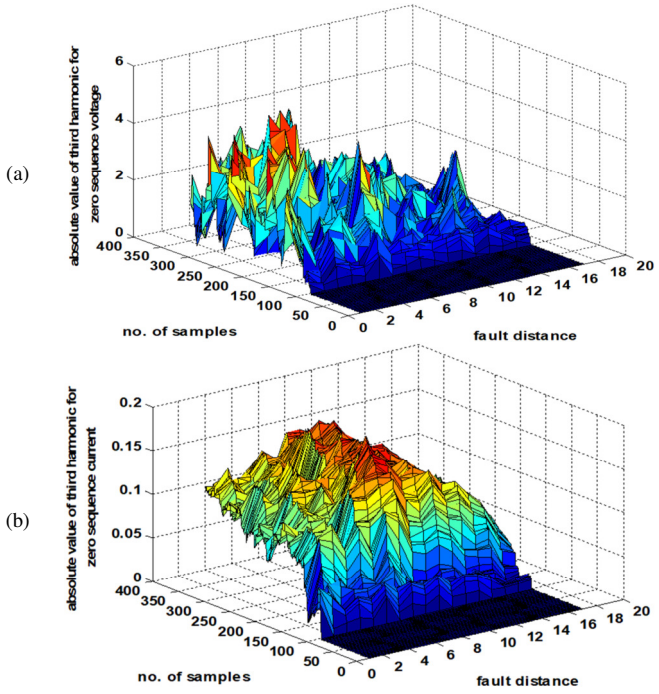

Fig. 11. Performance profile of the 3rd harmonic of the zero sequence component of (a) voltage waveform (b) current waveform for HIF with 1000Ω *Rf*.

B. Load Switching

If a switching operation occurs on a feeder, the higher harmonics associated with the switching transients may cause maloperation of the protection system, potentially resulting in the detection of a high impedance fault. Figure 12 demonstrates the variation of the summated values of the D1 coefficient of voltage and current waveforms for the switching off of Section 12-19 as depicted in Figure 2, occurring at 0.6 s. The maximum summated values of voltage and current waveforms are 35 V and 7.3 A, respectively, for the switching of Section 12-19. In contrast, based on the results from the previous subsections, it can be concluded that the minimum summated values of voltage and current waveforms under different HIFs equal 27.8 V and 0.51 A, respectively. Therefore, the first criterion of the proposed detection approach is unfortunately met under this load switching case, where the monitored values exceed this criterion's threshold value. However, the security of the proposed approach is maintained by monitoring the 3rd harmonic for the zero-sequence component of voltage and current waveforms. Figure 13 demonstrates the variation of the 3rd harmonic of the zero-sequence component of voltage and current waveforms for the switching off of Section 12-19 occurring at 0.6 s. On the other hand, based on the results from the previous subsections, the minimum difference between the new 3rd harmonic magnitude during HIF and the average value of the stored 3rd harmonic magnitude of the zero-sequence component of voltage and current waveforms are 0.0822 V and 0.0125 A, respectively. Additionally, the 3rd harmonic magnitude for voltage and current waveforms for the zero-sequence component of voltage and current waveforms remains approximately unchanged due to the switching of feeder Section 12-19. Consequently, the change in the 3rd harmonic magnitude can distinguish between load switching and HIF. The threshold values (2/3 of the corresponding minimum values under the occurrence of HIFs) are acceptable, as they are referenced to the secondary side of the current and voltage transformers with a ratios of 5:100 and 110:11000, respectively. In all tests, the HIF detection approach has proven to be both selective and reliable.

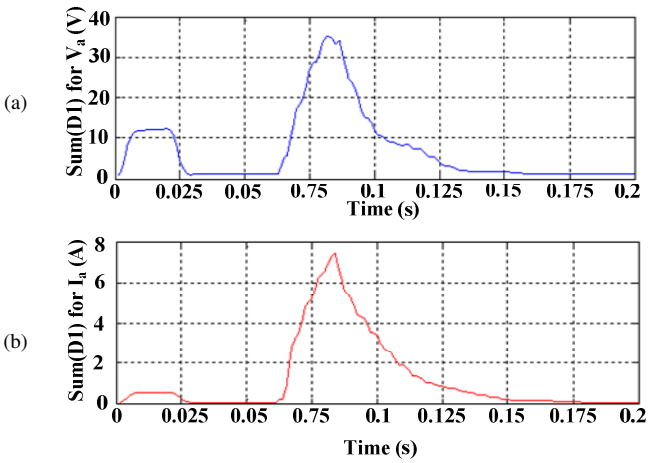

Fig. 12. Variation of the summated values of coefficient D1 of (a) voltage waveform (b) current waveform for switching off Section 12-19.

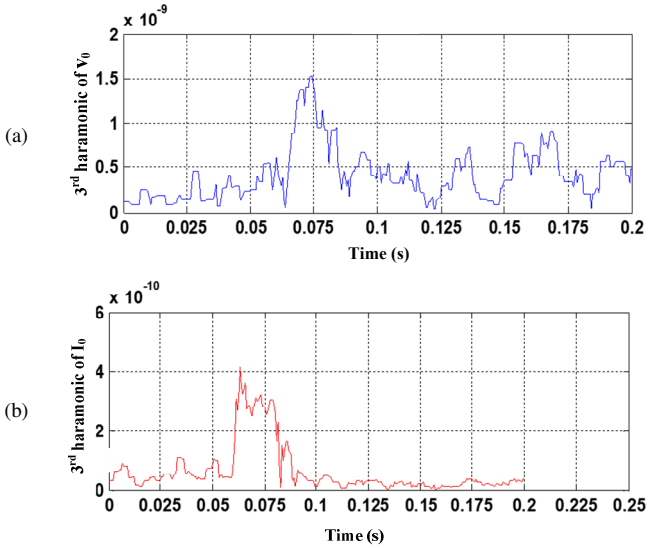

Fig. 13. Variation of the 3rd harmonic component of the zero sequence of (a) voltage waveform (b) current waveform for switching off Section 12-19.

V. EXPERIMENTAL VALIDATION

The proposed fault detection method was validated experimentally based on conducted fault cases in the real field in an Egyptian distribution system. The conducted experiments were authorized by the South-Delta Distribution system operator. One of the outgoing feeders from the distributor located in Shebin Elkom, Menoufia governorate was selected for the performed experiments. Figure 14(a) shows a single line diagram for the medium voltage distribution panels at which the voltage and current signals are captured. Figure 14(b) shows photos of the medium voltage panels where the data are captured and the implementation of the high impedance fault in the real field. The ratios of the already included medium voltage transformers in the distribution system are 11/0.11 kV and 100/5 A for the voltage and current transformers, respectively. For capturing the signals, additional Hall effect transducers were connected to the secondaries of the medium voltage measuring transformers as indicated in the Figure. dSPACE DS1104 R&D controller board was utilized for performing the capturing process of the signals. The outputs of the Hall effect were connected to the associated connector board into the analog-to-digital converters inputs. The utilized Hall effect transducers were adopted and configured with interface circuit and enclosed in a box as shown in Figure 14(c). These transducer boards ensure protection against any surges that could potentially damage the controller. The three-phase voltages were measured from the voltage transformer connected at the incoming feeder and the three-phase currents were measured from the current transformer connected with the selected outgoing feeder.

The HIF condition was implemented in real field as shown in Figure 14(b). The implemented fault is approximately 1.5 km from the panels. The feeder was initially disconnected to set up the fault. The feeder was then re-energized, creating a closing-on-to-fault condition, allowing for real-time monitoring

of voltages and currents. The captured signals were stored on a personal computer and were plotted in MATLAB. The results provide the evidence that the proposed protection is reliable against recorded HIFs, as in Figures 15-16, where the recorded 3rd harmonic components of the zero-sequence components of current and voltage waveforms are more than the corresponding threshold values.

To better clarify why the 3rd harmonic is the selected component of the zero-sequence current, signal analysis was performed using DFT on the other harmonic components of the captured data. The results indicate that the 3rd harmonic is more dominant in distinguishing such fault cases compared to other harmonic components, as shown in Figures 15(c)-(d) for the current and voltage signals, respectively.

(a)

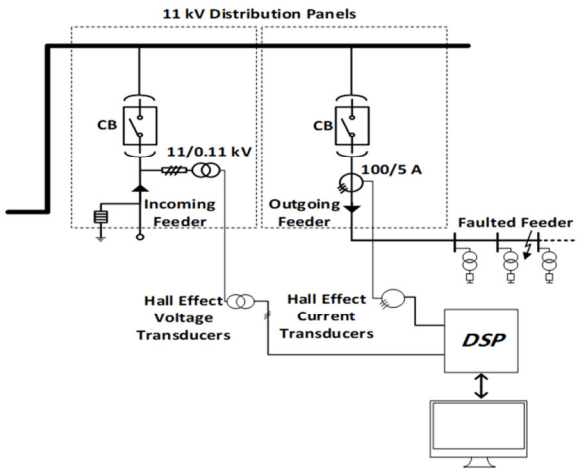

(b)

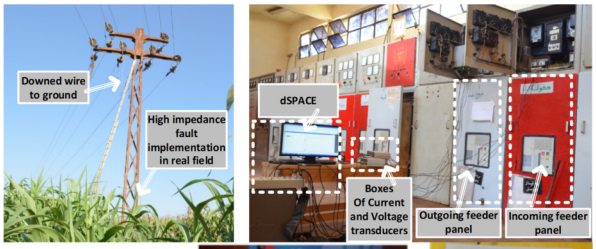

(c)

Fig. 14. Implementation of the HIF fault method.

(a)

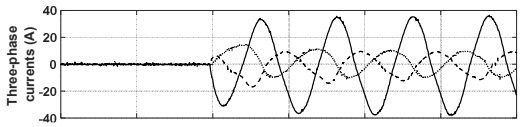

(b)

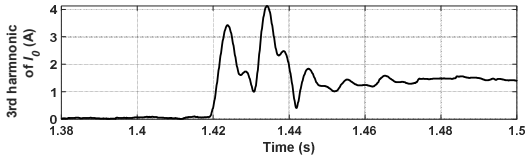

(c)

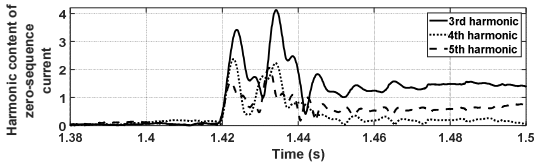

Fig. 15. Actual recordings of three phase currents and the obtained 3rd harmonic of the zero-sequence component under a HIF fault.

(a)

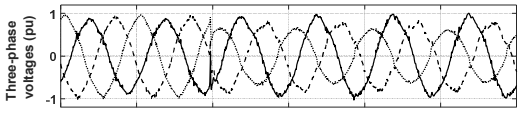

(b)

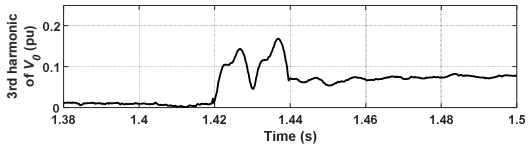

(c)

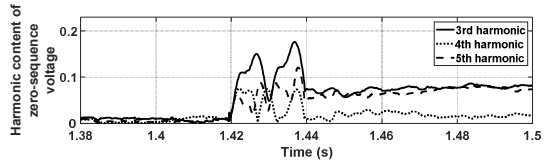

Fig. 16. Actual recording of three phase voltages and the obtained 3rd harmonic of the zero-sequence component under a HIF fault.

VI. CONCLUSIONS

A new method for detecting high impedance faults in medium voltage distribution networks is introduced in this paper. This method effectively distinguishes between high-impedance arcing faults and switching events. In conjunction with the conventional wavelet transform algorithm, the key to this discrimination lies in analyzing the variations of the third harmonic of both current and voltage in the zero-sequence. Switching events have been observed to lack changes in the third harmonic zero sequence components. In contrast, high-impedance arcing faults consistently exhibit alterations in these component magnitudes compared to pre-fault conditions. Furthermore, an optimal mother wavelet was meticulously selected based on extensive research. The algorithm demonstrates robustness in handling diverse fault conditions and exhibits clear discrimination capabilities between high impedance faults and switching events. Additionally, the proposed technique has been experimentally validated for reliability.

ACKNOWLEDGMENT

The authors extend their appreciation to the Deanship of Scientific Research at Northern Border University, Arar, KSA for funding this research work through the project number "NBU-FFR-2024-1250-03."

REFERENCES

[1] E. M. Esmail, M. M. Elgamasy, T. A. Kawady, A.-M. I. Taalab, N. I. Elkalashy, and M. A. Elsadd, "Detection and experimental investigation of open conductor and single-phase earth return faults in distribution systems," *International Journal of Electrical Power & Energy Systems*, vol. 140, Sep. 2022, Art. no. 108089, https://doi.org/10.1016/j.ijepes.2022.108089.

[2] M. S. Zaky, H. E. Ahmed, M. Elsadd, and M. Elgamasy, "Protection of HVDC Transmission Systems for Integrating Renewable Energy Resources," *Engineering, Technology & Applied Science Research*, vol. 13, no. 6, pp. 12237–12244, Dec. 2023, https://doi.org/10.48084/etasr.6463.

[3] N. I. Elkalashy *et al.*, "Earth fault distance estimation using travelling waves provided with triacs-based reclosing in distribution networks," *IET Renewable Power Generation*, vol. 15, no. 1, pp. 43–57, 2021, https://doi.org/10.1049/rpg2.12004.

[4] B. K. Ponukumati, A. K. Behera, L. Subhadarshini, P. Sinha, M. K. Maharana, and A. V. P. Kumar, "Unbalanced Distribution Network Cross-Country Fault Diagnosis Method with Emphasis on High-Impedance Fault Syndrome," *Engineering, Technology & Applied Science Research*, vol. 14, no. 2, pp. 13517–13522, Apr. 2024, https://doi.org/10.48084/etasr.6917.

[5] A. Ghaderi, H. L. Ginn, and H. A. Mohammadpour, "High impedance fault detection: A review," *Electric Power Systems Research*, vol. 143, pp. 376–388, Feb. 2017, https://doi.org/10.1016/j.epsr.2016.10.021.

[6] N. I. Elkalashy, M. Lehtonen, H. A. Darwish, A.-M. I. Taalab, and M. A. Izzularab, "A novel selectivity technique for high impedance arcing fault detection in compensated MV networks," *European Transactions on Electrical Power*, vol. 18, no. 4, pp. 344–363, 2008, https://doi.org/10.1002/etep.179.

[7] T. NengLing and C. JiaJia, "Wavelet-based approach for high impedance fault detection of high voltage transmission line," *European Transactions on Electrical Power*, vol. 18, no. 1, pp. 79–92, 2008, https://doi.org/10.1002/etep.169.

[8] I. Baqui, I. Zamora, J. Mazón, and G. Buigues, "High impedance fault detection methodology using wavelet transform and artificial neural networks," *Electric Power Systems Research*, vol. 81, no. 7, pp. 1325–1333, Jul. 2011, https://doi.org/10.1016/j.epsr.2011.01.022.

[9] K. Rai, F. Hojatpanah, F. Badrkhani Ajaei, and K. Grolinger, "Deep Learning for High-Impedance Fault Detection: Convolutional Autoencoders," *Energies*, vol. 14, no. 12, Jan. 2021, Art. no. 3623, https://doi.org/10.3390/en14123623.

[10] S. Kavaskar and N. K. Mohanty, "Detection of High Impedance Fault in Distribution Networks," *Ain Shams Engineering Journal*, vol. 10, no. 1, pp. 5–13, Mar. 2019, https://doi.org/10.1016/j.asej.2018.04.006.

[11] A. Aljohani and I. Habiballah, "High-Impedance Fault Diagnosis: A Review," *Energies*, vol. 13, no. 23, Jan. 2020, Art. no. 6447, https://doi.org/10.3390/en13236447.

[12] J. C. Huaquisaca Paye *et al.*, "High Impedance Fault Models for Overhead Distribution Networks: A Review and Comparison with MV Lab Experiments," *Energies*, vol. 17, no. 5, Jan. 2024, Art. no. 1125, https://doi.org/10.3390/en17051125.

[13] M. Kizilcay and P. La Seta, "Digital simulation of fault arcs in medium-voltage distribution networks," in *15th Power Systems Computation Conference*, Liege, Belgium, Aug. 2005, pp. 1–7.